Elutriation from Fluidized BEDS

Renaud Ansart, Hervé Neau, Philippe Accart, Alain de Ryck, Olivier Simonin

ELUTRIATION FROM FLUIDIZED BEDS: COMPARISON BETWEEN EXPERIMENTAL MEASUREMENTS AND 3D SIMULATION RESULTS

Renaud Ansart[1 2], Hervé Neau [1 2], Philippe Accart[3 4]
Alain de Ryck[3 4] and Olivier Simonin[1 2]
[1] Université de Toulouse; INPT, UPS; IMFT ; F-31400 Toulouse, France
[2] CNRS; Institut de Mécanique des Fluides de Toulouse; F-31400 Toulouse, France
[3] Université de Toulouse; Mines Albi; RAPSODEE; F-81013 Albi, France
[4] CNRS, Centre RAPSODEE, Campus Jarlard, F-81013 Albi, France
ansart@imft.fr, simonin@imft.fr

ABSTRACT

This paper presents comparisons between experimental measurements and unsteady three-dimensional numerical simulations performed by an unstructured parallelized CFD multiphase flow code of elutriation and transport of mono-dispersed glass beads type B and A/B in a fluidized bed. These comparisons show a satisfactory agreement between experimental measurements and numerical predictions. The numerical results also show a strong dependence on the mesh size, especially for fine particles. A model accounting for influences of meso-scales structures on overall bed hydrodynamics, which are not resolved by coarse mesh simulations, is applied. Results obtained with the model show improvements for the dense fluidized bed and even for a transport step.

INTRODUCTION

Gas-solid fluidized beds are used in a wide range of industrial applications such as coal combustion, catalytic polymerization and uranium fluoridation. Many of the fluidized bed industrial processes involve poly-dispersed powder and even multi-species of powders. In bubbling fluidized bed combustion and catalytic cracking, elutriation is a major cause of inefficiency, while it could be highly desirable in specific case. Whether the intention is to minimize or to promote elutriation, the involved phenomena must be properly known if the process has to be efficiently controlled.

Numerical simulation is becoming an efficient approach to study the separation and entrainment processes observed in an industrial fluidized bed. In the literature, there is a lack of experimental data to validate CFD simulations of these phenomena. Thus, a joint experimental and numerical project between RAPSODEE Centre and IMFT was initiated. The object of this paper is to present comparisons between three-dimensional numerical simulation predictions and experimental data of particle gas pressure drop and entrainment in a fluidized bed.

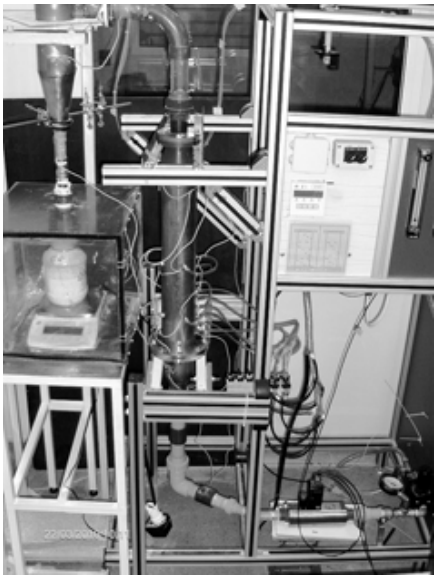

Fig. 1: Experimental set up.

Particle properties	**Fine**	**Coarse**
Solid mass (kg)	2.5	2.5
Density $(\mathrm{kg/m^3})$	2470	2470
Diameter d_{50} $(\mu\mathrm{m})$	84	213
Span=$\frac{d_{90}-d_{10}}{d_{50}}$	0.38	0.414
V_t $(\mathrm{m \cdot s^{-1}})$	0.41	1.51
U_{mf} $(\mathrm{m \cdot s^{-1}})$	$5 \cdot 10^{-3}$	$36 \cdot 10^{-3}$

Table. 1: Powder properties.

EXPERIMENTAL SET UP

The column in the laboratory experimental set up was 10 cm in diameter and $59\ \mathrm{cm}$ high (Fig. 1) and was fitted with a conical outlet. The column material was stainless steel to avoid electrostatic charge (Ansart et al. (1)). The bronze distributor had a pressure drop of $6\ \mathrm{kPa}$ at a superficial gas velocity of $0.18\ \mathrm{m \cdot s^{-1}}$. Fluidizing air was supplied by a Brooks smart mass flow meter and controllers 5853S with an accuracy of $\pm 0.7\ \%$ of the rate and $\pm 0.2\ \%$ of full scale ($2.32\ \mathrm{m \cdot s^{-1}}$).

The process was divided into two parts: the first allowed the fluidization of particles by a homogeneous superficial gas velocity ($V_{f1} < V_t$), in order to obtain a bubbling fluidized bed regime. According to a linear ramp-up of $5\ \mathrm{s}$ during the second part, the fluidization velocity was increased to entrain the particles ($V_{f2} > V_t$). The particles entrained were collected through a vessel at the outlet of a cyclone. The mass of particles collected was continuously weighed during the process with a resolution time of $1\ \mathrm{s}$ and an accuracy of $0.01\ \mathrm{g}$. Pressure variations along the pipe were monitored by severals sensors located every $1.5\ \mathrm{cm}$. Honeywell DC pressure instrumentation was used with an accuracy of $\pm 0.25\ \%$ of full scale. The resolution time was $0.1\ \mathrm{s}$. The measurement of gas pressure on the wall was made through an $8\ \mathrm{mm}$ diameter opening with a filter.

The powder was glass beads with properties described in Table 1. For $2.5\ \mathrm{kg}$ of solid mass, the bed at rest in the column is approximatively $21\ \mathrm{cm}$. Two particle sizes called fine (Geldart type A/B) and coarse (Geldart type B) were used. The mean diameters of powder were determined using a Mastersizer 2000 with $1.5\ \mathrm{bar}$ of dispersion. The bulk material was sieved to ensure an almost mono-dispersed distribution. The terminal settling velocity V_t of the particle was calculated by the expression of the drag coefficient, Equation (5). According to Re_{mf}, an estimation of minimum fluidization velocity U_{mf} was computed using the expression recommended by Wen and Yu:

$$Re_{mf} = (33.7^2 + 0.0408 \frac{\rho_g(\rho_p - \rho_g)d_p^3 g}{\mu_g^2})^{0.5} - 33.7 \qquad U_{mf} = \frac{Re_{mf}\mu_g}{\rho_p d_p}. \qquad (1)$$

MATHEMATICAL MODEL

Simulations were carried out using an Eulerian n-fluid modeling approach for poly-dispersed fluid-particle flows implemented in the NEPTUNE_CFD software which was developed and implemented by IMFT (Institut de Mécanique des Fluides de Toulouse). This software is a multiphase flow code developed in the framework of the NEPTUNE project, financially supported by CEA (Commissariat à l'Énergie Atomique), EDF (Électricité de France), IRSN (Institut de Radioprotection et de Sûreté Nucéaire) and AREVA.

In the proposed modeling approach, the mean transport equations (mass, momentum and fluctuant kinetic energy) are solved for each phase and coupled through interphase transfer terms. These equations are derived by phase ensemble averaging weighted by the gas density for the continuous phase and by using kinetic theory of granular flows supplemented by fluid and turbulence effects for the dispersed phase (Balzer et al. (2), Gobin et al. (3)). In the following development, subscript $k = g$, refers to the gas phase and $k = p$ refers to the particle phase. The mass balance equation is:

$$\frac{\partial}{\partial t}\alpha_k\rho_k + \frac{\partial}{\partial x_i}\alpha_k\rho_k U_{k,i} = 0, \tag{2}$$

where α_k is the k^{th} phase volume fraction, ρ_k the density and $U_{k,i}$ the i^{th} component of the velocity. In equation (2), the right-hand-side is equal to zero without mass transfer. The mean momentum transport equation for the phase k is written:

$$\alpha_k\rho_k\left[\frac{\partial U_{k,i}}{\partial t} + U_{k,j}\frac{\partial U_{k,i}}{\partial x_j}\right] = -\alpha_k\frac{\partial P_g}{\partial x_i} + \alpha_k\rho_k g_i + I_{k,i} + \frac{\partial}{\partial x_j}\left[-\alpha_k\rho_k\left\langle u'_{k,i}u'_{k,j}\right\rangle + \Theta_{p,ij}\right], \tag{3}$$

where $u'_{k,i}$ is the fluctuating part of the instantaneous velocity of phase k, P_g is the mean gas pressure, g_i the i^{th} component of the gravity acceleration and $I_{k,i}$ the mean gas particle interphase momentum transfer without the mean gas pressure contribution. Finally, $\Theta_{k,ij}$ is for $k = g$ the molecular viscous tensor and for $k = p$ the collisional particle stress tensor. Due to the large particle to gas density ratio, only the drag force was assumed to be acting on the particles. Hence, the mean gas-particle interphase momentum transfer can be written:

$$I_{p,i} = -I_{g,i} = -\alpha_p\rho_p\frac{V_{r,i}}{\tau_{gp}^F} \quad \text{with} \quad \frac{1}{\tau_{gp}^F} = \frac{3}{4}\frac{\rho_g}{\rho_p}\frac{\langle|\mathbf{v}_r|\rangle}{d_p}C_{d,\text{WY}}. \tag{4}$$

with $C_{d,\text{WY}}$ given by Wen $\&$ Yu's correlation:

$$C_{d,WY} = \begin{cases} \frac{24}{Re_p}\left(1 + 0.15Re_p^{0.687}\right)\alpha_g^{-1.7} & Re_p < 1000 \quad Re_p = \alpha_g\frac{\rho_g\langle|\mathbf{v}_r|\rangle d_p}{\mu_g} \\ 0.44\ \alpha_g^{-1.7} & Re_p \geq 1000 \end{cases} \tag{5}$$

The mean relative velocity $V_{r,i}$ between gas and particle is expressed in terms of the mean gas velocity, mean particle velocity and drift velocity. In equation (3), the collisional particle stress tensor is derived in the frame of the kinetic theory of granular media (Boelle et al. (4)).

For the gas turbulence, a standard $k-\varepsilon$ model extended to the multiphase flows accounting for additional source terms due to the interfacial interactions was used. For the dispersed phase, a coupled transport equation system is solved on particle fluctuating kinetic energy and fluid-particle fluctuating velocity covariance ($q_p^2 - q_{fp}$).

In this paper, the influence of mesh size on the numerical predictions was studied. The mesh size required to fully resolve all of the fine-scale structures decreased as a function of the mean particle relaxation timescale (Parmentier et al. (5)). Because of limited computational resources, a filtered approach can be used to model the drag term accurately (Agrawal (6)). In the framework of a filtered approach for gas-solid flows, Parmentier et al. (7) proposed that the filtered drag can be modeled by:

$$\overline{\left(\frac{\alpha_p \rho_p}{\tau_{gp}^F} V_{r,i}\right)} = \frac{\overline{\alpha}_p \rho_p}{\widetilde{\tau}_{gp}^F} \left(\delta_{ij} + h(\overline{\alpha}_p) K_{ij} f(\Delta_G^*)\right) \widetilde{V}_{r,j}, \tag{6}$$

where $\widetilde{V}_{r,j} =$ is the resolved relative velocity. $K_{ij} = \delta_{ij} K_h + \delta_{i3}\delta_{j3}(K_v - K_h)$, the model coefficient is the same in x and y direction (K_h and K_v are determined by a dynamic adjustment performed by a second filter). $h(\overline{\alpha}_p) = -\sqrt{u}\ (1-u)^2\ (1 - 1.88\ u + 5.16\ u^2)$, where $u = \overline{\alpha}_p / \alpha_m$ et $\alpha_m = 0.64$ is the maximum compacting. The forms of the h and f functions are derived from a highly-resolved simulation of mono-dispersed gas-solid flow. The function f is modeled as the following equation:

$$f(\Delta_G^*) = \frac{{\Delta_G^*}^2}{a^2 + {\Delta_G^*}^2} \quad \text{with} \quad \Delta_G^* = \frac{\Delta_G}{\tau_p^{St}\sqrt{gL}}. \tag{7}$$

where $a = 0.084$, Δ_G^* is a dimensionless mesh size, Δ_G the cube root of the cell volume, L the bed diameter and τ_p^{st} stokes relaxation time.

NUMERICAL PARAMETERS

To study the influence of mesh refinement, we used three 3D meshes based on O-grid technique were used. The reference mesh contained 428 451 hexahedra with approximately $\Delta_x = \Delta_y = \Delta_z = 3.7\,\mathrm{mm}$. The mesh was uniformly refined by a factor of 1.5 which consisted of 1 477 060 cells. The coarse mesh was made up of 123 816 cells constructed from the reference mesh by coarsening by a factor of 1.5. The numerical simulations were performed on parallel computers with 8 cores for the coarse mesh, 64 cores for the reference mesh and 128 cores for the fine mesh, because of mesh size and physical time needed (Neau et al. (8)).

At the bottom ($z = 0$), the fluidization grid was an inlet for the gas, with an imposed superficial velocity corresponding to the fluidization velocity v_f, and a wall for the particles. At the top of the fluidized bed, a free outlet for both the gas and the particles was defined. The wall-type boundary condition was friction for the gas and a no-slip for the particle. Fede et al. (9) have shown that the gas pressure drop predictions are improved with a no-slip boundary condition for the mean particle velocity and zero-flux condition for the mean particle agitation q_2^p.

RESULTS AND DISCUSSION

First of all, a comparison between the numerical predictions for the coarse particles and the experimental results was obtained. Then, the same comparison was carried

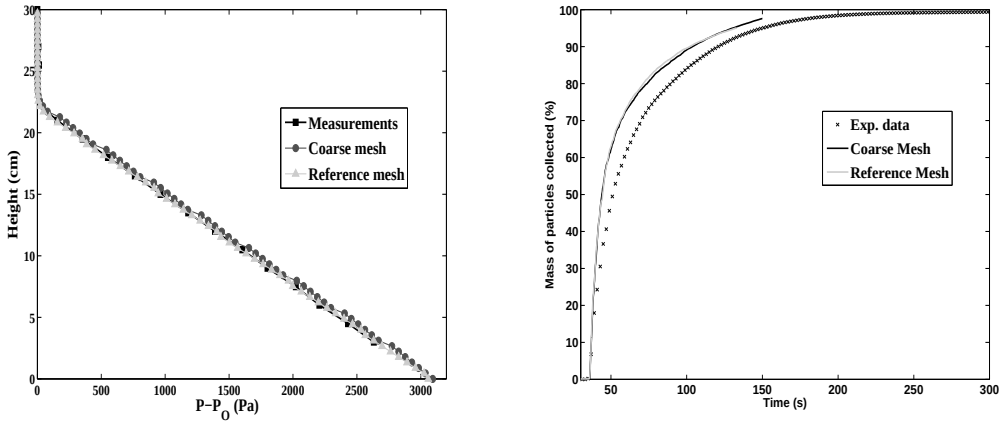

(a) Wall distribution of the mean gas pressure.

(b) Mass of particles collected.

Fig. 2: Comparison between experimental data and numerical simulation predictions for coarse particles. In the left plot the data were obtained during the bubbling step $V_{f1} = 2.5\ U_{mf}$ and in the right plot during the entrainment step $V_{f2} = 1.03\ V_t$.

out for the results of fine particles. In the experiments, the particle phase was slightly poly-dispersed (span ≈ 0.4). However, the numerical simulations were carried out with a monodisperse particle distribution having a median diameter equal to d_{50}.

Coarse particles

Gas pressure drop along the wall during the bubbling phase and the mass of particles collected obtained by numerical predictions, for the coarse and reference mesh sizes, were compared with the experimental measurements. To study the wall gas pressure drop during the bubbling step, the numerical simulations were carried out as follows: at $t = 0$ the fluidized bed was filled up with a uniform solid mass fraction according to the experimental solid mass. A transitory step takes place for $t \in [0\ \mathrm{s},\ 20\ \mathrm{s}]$ corresponding to the destabilization of the fluidized bed. Then, the statistics were computed for $t \in [20\ \mathrm{s},\ 60\ \mathrm{s}]$ insuring a statistical convergence.

As Fig. 2 shows, the mesh refinement had no effect on the bed expansion or the mass of particles entrained for the coarse particles (type B). The coarse mesh was sufficient to predict bed dynamics, and no further mesh refinement was needed. Moreover, a very good agreement between numerical predictions of the wall gas pressure drop and the experimental data during the bubbling step ($V_{f1} = 2.5\ U_{mf}$), Fig. 2(a), was obtained. Above the bed particles, the gradient of gas pressure was equal is negligible for the numerical results and for the experimental measurements. Inside the bed, both distributions were linear. The numerical results predicted the same bed height as the experimental data.

Fig. 2(b) shows the evolution of the mass of particles collected during the entrainment step ($V_{f2} = 1.03\ V_t$). A good agreement between the experimental measurements of the mass flow rate of coarse particles and the numerical results was obtained. Indeed, at the start of the entrainment process the flux of particles was slightly overestimated, and during the following progress of the process the numerical predictions of the flux were very close to the measurements.

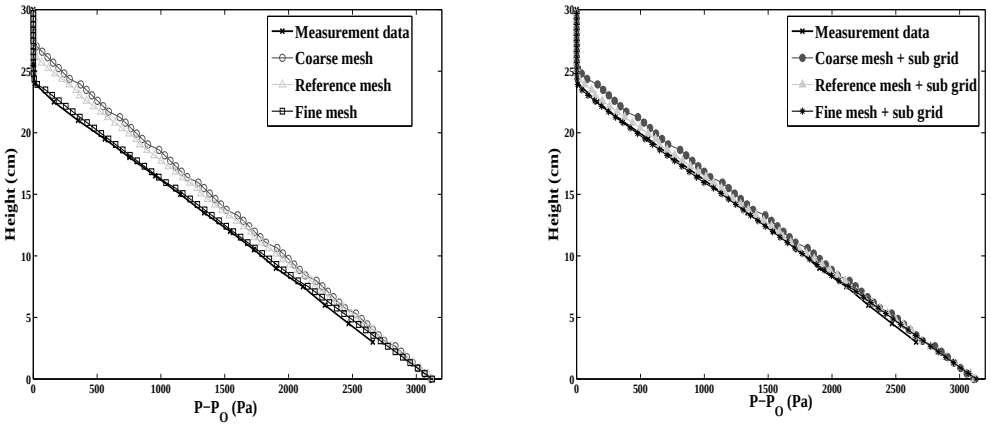

(a) Effect of mesh size.

(b) Effect of sub-grid model for drag force.

Fig. 3: Comparison between experimental data and numerical simulation predictions of wall mean gas pressure for fine particles during the bubbling step. $V_{f1} = 5\ U_{mf}$.

Fine particles

For fine particles, the numerical simulations were performed on three mesh sizes. Fig. 3(a) shows the wall distribution of time averaged gas pressure, during the bubbling step ($V_{f1} = 5\ U_{mf}$), for the experimental measurements and for the numerical predictions. As shown, mesh refinement had a strong effect on the numerical results for the fine particles. For the coarse and reference mesh sizes, the bed expansion was overestimated. Only, the fine mesh case was able to predict a similar wall gas pressure as the experimental measurements, and to correctly estimate the bed height. The structures of the gas-particle fluidized bed were not able to be resolved by the coarse and reference mesh simulations and they had a drastic influence on the macroscopic flow. To account for the effect of unresolved structures on the macroscopic behavior in the coarse and reference mesh sizes, the sub-grid model described before was used to model the effective drag term.

The Fig. 3(b) shows that the wall gas pressure drop predictions are greatly improved by using the sub-grid model. With the sub-grid model, the bed height was almost independent of the mesh size. A satisfactory agreement was obtained between the numerical predictions (fine grid and large grid with sub-grid model) and experimental measurements of the bed height, Table 2. The mean bed height was defined as the height where the gas pressure distribution slope was modified.

The Fig. 4 shows the mass of fine particles collected during the entrainment step ($V_{f2} = 1.53\ V_t$). In the bubbling phase, mesh refinement had a strong effect on the mass flow rate of particles entrained. Comparisons with the fine mesh simulation results showed that the coarse and reference mesh simulations overestimated the mass flow rate of the particles entrained. With the sub-grid model, the numerical simulations were approaching to the experimental measurements.

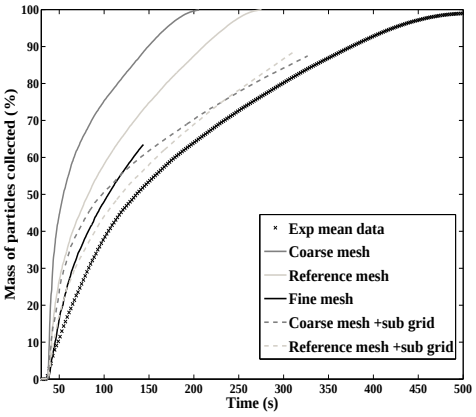

Fig. 4: Mass of fine particles collected during the entrainment step. $V_{f2} = 1.53\ V_t$.

	Bed height (cm)
Coarse mesh	27
Reference mesh	26.2
Fine mesh	24.1
Coarse mesh + sub-grid	24.5
Reference mesh + sub-grid	24.2
Fine mesh + sub-grid	23.6
Exp. data	24.2

Table. 2: Time-averaged bed height.

The simulation for the reference mesh with sub-grid model appeared to give similar results as with the simulation of fine mesh but with less expensive computational resources. As for the coarse particles, the flux of particles at the start of the process was slightly overestimated, and was similar to the experimental measurements for the following test duration.

CONCLUSION

An experimental test unit was designed and built to study particle separation and entrainment in a fluidized bed by measuring the gas pressure along the column and the mass of particles leaving the column. A three dimensional, unsteady numerical predictions was carried out with the unstructured parallelized CFD multiphase flow NEPTUNE_CFD were compared with experimental measurements.

Comparisons were obtained for two types of particles (B and A/B). The numerical predictions for type A/B have strong dependency on the mesh size. To account for the effect of unresolved structures on the macroscopic behavior for coarse grid simulations, a sub-grid model was used to model the drag term. Accordingly, the numerical results were greatly improved and were in good agreement with the fine grid simulation. Coarse numerical simulations with the sub-grid model were hugely much less expensive from the point of view of the computational resources. The numerical predictions of the bed height and of the entrainment rate were in good agreement with experimental measurements. The next step of this study is to focus on the elutriation of a mixture of fine and coarse particles.

ACKNOWLEDGMENTS

This work was granted access to the HPC resources of CINES under the allocation 2010-026012 made by GENCI (Grand Equipement National de Calcul Intensif) and CALMIP (Centre de Calcul Midi-Pyrénées) under the allocation P0111.

NOTATION

$C_{d,WY}$	Wen 'n Yu drag coefficient	V_r	relative velocity
d_p	particle diameter	V_t	terminal settling velocity
g	gravitational constant	$u'_{k,i}$	fluctuating velocity of phase k
P_g	mean gas pressure	α_k	volume fraction of phase k
q_p^2	mean particle agitation	Δ_G^*	dimensionless mesh size
Re_p	particle Reynolds number	Δ_G	cube root of the cell volume
$U_{k,i}$	mean velocity of phase k	μ_g	gas viscosity
U_{mf}	minimum fluidization velocity	ρ_k	density of phase
V_f	superficial gas velocity	τ_{gp}^F	mean gas-particle relaxation timescale

REFERENCES

1. Ansart, R., Neau, H., Accart, P., de Ryck, A. and Simonin, O. (2010). "Separation and Taking Off in a Fluidized Bed: Comparison between Experimental Measurements and Three-dimensional Simulation Results", Proceedings of 7^{th} International Conference on Multiphase Flows, Florida USA.

2. Balzer, G. and Boelle, A. and Simonin, O. (1995). "Eulerian Gas-Solid Flow Modelling of Dense Fluidized Bed", FLUIDIZATION VIII, Proc. International Symposium of the Engineering Foundation, J.F. Large and C. Laguérie (Editors).

3. Gobin, A., Neau, H., Simonin, O., Llinas, J.R. and Reiling, V. and Sélo, J.L. (2003). "Fluid Dynamic Numerical Simulation of a Gas Phase Polymerization Reactor", Int. J. for Num. Methods in Fluids, 43, 1199-1220.

4. Boelle, A., Balzer, G. and Simonin, O. (1995). "Second-order prediction of the prediction of the particle-phase stress tensor of inelastic spheres in simple shear dense suspensions", In Gas-Particle flows, Vol. 228, ASME FED. 9-18.

5. Parmentier, J.F., Simonin, O. and Delsart O. (2008). "A numerical study of fluidization behavior of Geldart B, A/B and A particles using an eulerian multifluid modeling approach", 9^{th} International Conference on circulating fluidized beds. Hamburg, Germany.

6. Agrawal, K., Loezos, P., Syamlal, M. and Sundaresan, S. (2001). "The Role of Mesoscales Structures in Rapid Gas-solid Flows", J. Fluid Mech., 445, 151-185.

7. Parmentier, J.F., Simonin, O. and Delsart O. (2010). "A functional subgrid drift velocity model for filtered drag prediction in dense fluidized bed", Submitted to AIChE Journal.

8. Neau, H., Laviéville, J. and Simonin, O. (2010). "NEPTUNE_CFD high parallel computing performances for particle laden reactive flows", Proceeding 7^{th} International Conference on Multiphase Flows, Florida USA.

9. Fede, P., Moula, G., Ingram, T. and Simonin, O. (2009). "3D numerical simulation and pept experimental investigation of pressurized gas-solid fluidized bed hydrodynamic", Proceedings of ASME 2009 Fluids Engineering Division Summer Meeting. ASME.